

MALDI FTICR IMS of Intact Proteins: Using Mass Accuracy to Link Protein Images with Proteomics Data

Jeffrey M. Spraggins,^{1,2} David G. Rizzo,^{2,3} Jessica L. Moore,^{2,3} Kristie L. Rose,^{1,2}
Neal D. Hammer,⁴ Eric P. Skaar,^{4,5} Richard M. Caprioli^{1,2,3,6}

¹Department of Biochemistry, Vanderbilt University School of Medicine, Nashville, TN 37205, USA

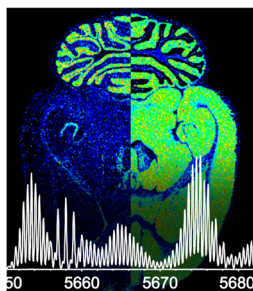
²Mass Spectrometry Research Center, Vanderbilt University School of Medicine, Nashville, TN 37232, USA

³Department of Chemistry, Vanderbilt University, Nashville, TN 37235, USA

⁴Department of Pathology, Microbiology and Immunology, Vanderbilt University School of Medicine, Nashville, TN 37232, USA

⁵U.S. Department of Veterans Affairs, Tennessee Valley Healthcare System, Nashville, TN 37212, USA

⁶Departments of Pharmacology and Medicine, Vanderbilt University School of Medicine, Nashville, TN 37232, USA



Abstract. MALDI imaging mass spectrometry is a highly sensitive and selective tool used to visualize biomolecules in tissue. However, identification of detected proteins remains a difficult task. Indirect identification strategies have been limited by insufficient mass accuracy to confidently link ion images to proteomics data. Here, we demonstrate the capabilities of MALDI FTICR MS for imaging intact proteins. MALDI FTICR IMS provides an unprecedented combination of mass resolving power ($\sim 75,000$ at m/z 5000) and accuracy (<5 ppm) for proteins up to ~ 12 kDa, enabling identification based on correlation with LC-MS/MS proteomics data. Analysis of rat brain tissue was performed as a proof-of-concept highlighting the capabilities of this approach by imaging and identifying a number of proteins including N-terminally acetylated thymosin β_4 (m/z 4,963.502, 0.6ppm) and ATP synthase subunit ϵ (m/z 5,636.074, -2.3 ppm). MALDI FTICR IMS was also used to differentiate a series of oxidation products of S100A8 (m/z 10,164.03, -2.1 ppm), a subunit of the heterodimer calprotectin, in kidney tissue from mice infected with *Staphylococcus aureus*. S100A8 – M37O/C42O₃ (m/z 10228.00, -2.6 ppm) was found to co-localize with bacterial microcolonies at the center of infectious foci. The ability of MALDI FTICR IMS to distinguish S100A8 modifications is critical to understanding calprotectin's roll in nutritional immunity.

Keywords: FTICR MS, Imaging MS, MALDI, Proteomics, Mass accuracy, Top-down, Calprotectin, PTMs, *Staphylococcus aureus*, Nutritional immunity

Received: 25 February 2015/Revised: 20 March 2015/Accepted: 20 March 2015/Published Online: 23 April 2015

Introduction

Matrix-assisted laser desorption/ionization imaging mass spectrometry (MALDI IMS) enables the visualization of biomolecules in tissue by combining the sensitivity and selectivity of mass spectrometry with the spatially descriptive characteristics of classic histology. Originally described by Caprioli et al. [1], the technology has been applied to the analysis of a variety of analyte classes, including pharmaceuticals [2, 3],

metabolites [4], lipids [5], peptides [6, 7], and proteins [8, 9]. Briefly, MALDI IMS experiments are performed by cutting fresh frozen or fixed tissue into thin sections and flat-mounting them onto a target. The sample is then coated with a MALDI matrix, which assists in desorption and ionization of endogenous molecules. During acquisition, virtually defined regions of the tissue are irradiated by a laser in an array of discrete points generating a mass spectrum at each x,y coordinate. Typically, image spatial resolution is defined by the size of the laser spot on target and the spacing between the points in the array. Spectral intensities for a given ion are then plotted across the array, creating ion images that can be compared with stained images of the tissue providing an additional molecular dimension to classical histologic analysis. MALDI IMS of intact proteins is of particular interest because in a single

Electronic supplementary material The online version of this article (doi:10.1007/s13361-015-1147-5) contains supplementary material, which is available to authorized users.

Correspondence to: Jeffrey Spraggins; e-mail: jeff.spraggins@vanderbilt.edu

experiment it has the potential to spatially describe the many endogenous proteoforms of a given protein, the various molecular forms which a protein product of a single gene can take (e.g., genetic variations and post-translational modifications) [10]. However, protein imaging experiments are hindered by the inability to structurally identify observed peaks, inhibiting the contextualization of IMS results with biological processes.

Protein identification strategies fall into three general categories; bottom-up, top-down, and indirect identification. Bottom-up experiments involve enzymatic digestion of the protein mixture prior to analysis by mass spectrometry [11]. For imaging experiments, proteins are digested on tissue by applying an enzyme and performing hydrolysis in a way that preserves the spatial integrity of the proteins. Matrix is then applied, and both MS and MS/MS analyses are performed directly from tissue [12, 13]. Because MALDI ions tend to be singly charged, collision induced dissociation (CID) is often the method used for fragmentation. This approach can be advantageous because it extends the mass range of observable proteins by enzymatic digestion. Further, for most anatomic pathology examinations of biopsies, the tissue has been formalin fixed and paraffin embedded for preservation, and so bottom-up proteomics is the preferred procedure for analysis. The downside is that in practice, fragmenting peptides from tissue is hindered by the inability to effectively isolate ions from the considerable background signal and low fragmentation efficiencies for singly charged peptides. Additionally, performing bottom-up experiments in general may miss information regarding post-translational modifications (PTMs) if the modified peptide is not detected.

Top-down strategies [14] provide another approach for protein identification in IMS experiments. Here identifications are made through measurements of intact proteins followed by on-tissue MS/MS analysis. This approach is ideal for spatially describing the different proteoforms of endogenous proteins. However, similar to bottom-up experiments, on-tissue fragmentation of intact proteins is restricted by poor fragmentation efficiency for singly charged proteins. Moreover, because most ions produced by MALDI have low charge states, electron-based fragmentation mechanisms (e.g., electron transfer dissociation) are often ineffective. Although work has been done to increase the charge state of ions generated from tissue through supercharging matrices [15, 16] or “ESI-like” surface analysis techniques [17–21] (e.g., LAESI, DESI, and MALDESI), further development is needed to improve image quality and sensitivity.

Indirect identification is an alternative approach that uses secondary information such as mass accuracy and spatial localization to link separate IMS and proteomics experiments. Because differences in preferential ionization between ESI and MALDI often lead to different peptides being detected, a direct link can be made between the two experiments by performing the analysis on intact proteins. Typically, protein images are collected using a linear TOF MS to accommodate for the relatively high m/z range. Then, with a serial section, proteins are extracted and analyzed using either top-down or bottom-up

LC-ESI MS/MS based identification strategies. Protein extraction can be performed by homogenizing the entire section [22, 23] or by using spatially directed extraction technologies [24]. A major advantage of indirect identification is that it allows both the imaging and proteomics experiments to be operated under optimal conditions maximizing the sensitivity of both technologies. However, protein imaging using MALDI TOF MS does not provide the resolving power and mass accuracy necessary to correlate imaging data to proteomics experiments with high confidence. Mass accuracies for MALDI TOF measurements are particularly skewed when collecting data directly from tissue, which introduces sample height differences and can promote surface charging attributable to the insulating nature of many tissues. In practice, the mass accuracy of a MALDI TOF protein imaging experiment is limited to 20–100ppm, making identification based on mass accuracy unachievable. These negative sample surface effects on spectral quality are minimized when using decoupled mass analyzers such as FTICR, Orbitrap, and orthogonal TOF mass spectrometers.

Fourier transform mass spectrometers, such as Fourier transform ion cyclotron resonance (FTICR) [25] and orbital trapping (Orbitrap) [26, 27], provide the highest mass resolution and accuracy of all mass analyzers. For imaging experiments, these high performance instruments routinely produce ion images with mass resolving powers greater than 50,000 ($m/\Delta m_{50\%}$) and mass accuracies better than 5ppm [4, 28, 29]. These instruments are extremely valuable for tissue analysis where high resolving power is necessary to distinguish endogenous nominal isobars and high mass accuracy allows for more robust identification. Recently, accurate mass measurements (<5ppm) have been shown to greatly increase the reliability of peptide identification by dramatically reducing the number of false positive identifications for IMS experiments using indirect identification strategies [30, 31]. FT-based IMS in combination with LC-ESI MS/MS has also proven to be useful for small molecule [32] and lipid analysis [28]. Neither FTICR nor Orbitrap platforms have been used for MALDI IMS of intact proteins because FT-based platforms have traditionally been m/z range limited. However, modern instrumentation (source ion optics) and access to higher magnetic fields has dramatically improved the sensitivity and throughput of FTICR platforms at higher mass ranges.

Here we demonstrate intact protein images generated using MALDI FTICR MS. This approach provides an unprecedented combination of mass accuracy (<5ppm) and resolving power ($\sim 75,000$ at m/z 5000) for proteins up to ~ 12 kDa enabling identifications based on correlation with LC-based proteomics data to be made with high confidence. Additionally, we provide a case study demonstrating the capabilities of MALDI FTICR MS to elucidate multiple proteoforms of S100A8, a protein subunit of the heterodimer calprotectin, in kidney tissue of mice infected with *Staphylococcus aureus*. This work builds from our laboratories' previous studies of the inflammatory response in animal models of bacterial infection where the host subunits of calprotectin were found to localize to bacterial

abscesses [33–39]. Calprotectin is an abundant metal-binding protein that accounts for ~60% of the cytosolic protein content of neutrophils, the most abundant immune cell of vertebrates [40]. The protein contains a calcium-binding domain and two distinct histidine-rich motifs that are necessary to bind zinc and manganese [41]. The ability of calprotectin to chelate nutrient zinc and manganese is critical to the antimicrobial and antifungal properties of the protein [42, 43]. MALDI FTICR IMS allows for the spatial elucidation of previously unresolved modifications to S100A8 providing further insight into the molecular state of important host defense proteins at the host–pathogen interface.

Experimental

Materials

Acetic acid, trifluoroacetic acid (TFA), and 2,5-dihydroxyacetophenone (DHA) were purchased from Sigma-Aldrich Chemical Co. (St. Louis, MO, USA). HPLC-grade acetonitrile (ACN), ethanol, chloroform, trifluoroethanol, and Tris buffer were purchased from Fisher Scientific (Pittsburgh, PA, USA).

Animals

Fresh frozen rat brains were purchased from Pel-Freez Biologicals (Rogers, AR, USA). All in-house animal experiments were performed with approval by the Vanderbilt Institutional Animal Care and Use Committee. Six-week old female mice were anesthetized and retro-orbitally inoculated with *Staphylococcus aureus* (*S. aureus*). Systemic infection was allowed to progress for 6 to 9 d. Kidneys for imaging experiments were aseptically removed and flash-frozen using a mix of hexane and dry ice. Tissue for protein identification was removed and placed into sterile containers for homogenization.

MALDI IMS

Frozen tissue was sectioned to 10 μ m at –20°C using a Leica CM 3050S cryostat (Leica Microsystems, GmbH, Wetzlar, Germany). Sections were mounted onto conductive indium-tin-oxide coated slides (Delta Technologies). Tissue was washed to remove interfering lipids and salts in sequential washes of 70% ethanol (30s), 100% ethanol (30s), Carnoy fluid (6:3:1 ethanol: chloroform:acetic acid) (2min), 100% ethanol (30s), water with 0.2% TFA (30s), and 100% ethanol (30s). Slides were stored at –80°C until IMS analysis was performed. Matrix was applied using a TM Sprayer (HTX Technologies, Carrboro, NC, USA) with a 15mg/mL DHA in 8:1:1 acetone:water:acetic acid matrix solution. Other instrument parameters include a flow rate 0.15mL/min, nitrogen flow of 10psi, spray temperature of 30°C, four passes with offsets and rotations, a spray velocity of 1300mm/min, and 90% ACN as the pushing solvent.

Imaging experiments were performed using a 15T Bruker MALDI FTICR mass spectrometer (Bruker Daltonics,

Billerica, MA, USA). The instrument is equipped with an Apollo II dual MALDI/ESI ion source and a Smartbeam II 2kHz Nd:YAG (355nm) laser. All images were collected using the small laser setting (~50 μ m) with a pixel spacing of 75 μ m in both x and y dimensions. Data were collected from m/z 1000 to 15,000 with a resolving power of ~40,000 and ~75,000 at m/z 5000 for the brain and kidney analyses, respectively. Special tuning of the Funnel rf amplitude (190 Vpp), accumulation hexapole (1.4MHz, 1200 Vpp), transfer optics (1MHz, 310 Vpp), time of flight delay (2.5ms), and ICR cell (sweep excitation power: 43%) were required for high m/z analysis. External calibration was performed prior to analysis using CsI clusters. FlexImaging 4.1 (Bruker Daltonics) was used to visualize ion images. For comparison, linear MALDI-TOF data were collected using a Bruker Autoflex Speed (Bruker Daltonics).

Protein Purification

Rat brain was sectioned on a Leica cryostat and cerebrum was separated from cerebellum by a chilled razor blade. The cerebellum and cerebrum tissue sections were collected into corresponding pre-weighed Eppendorf tubes. At least 10 sections were combined into each tube before extraction was performed. An extraction solution composed of 25mM Tris (pH7.4), 50mM NaCl, and 0.25mM EDTA was made and approximately 350 μ L was pipetted into each tube. An ice-chilled Duall homogenizer was used to homogenize the tissues, with 15–20 homogenization strokes used to liquefy the samples. A 150 μ L aliquot of each homogenate was taken and 1.53 μ L of acetic acid and TFA were added. The samples were homogenized again using the tissue homogenizer and set on ice for 30min with intermittent vortexing to avoid sample aggregation. Homogenates were spun down at 20,000 $\times g$ for 15min and the supernatants collected. A Bradford assay (Thermo Scientific Pierce, Rockford, IL, USA) was used to quantify total protein concentration from each sample and the concentrations were adjusted to 2 μ g/ μ L with 0.1% formic acid for subsequent LC analysis.

Kidneys of *S. aureus* infected animals were homogenized using 1mL of phosphate buffered saline and a rolling pin. Cells were lysed by adding 0.5mL of 50% trifluoroethanol and centrifuged for 10min at 9g using Eppendorf Centrifuge 5415c. Protein was extracted from homogenates using 0.5mL of 60% acetonitrile and centrifuged for 10min at 6700 $\times g$. Supernatants from the extraction were saved and proteins were quantified using a Bradford Assay (Thermo Scientific Pierce). Extracted proteins were further fractionated by reversed-phase HPLC using a Waters 2690 Alliance Separations Module (Waters, Milford, MA, USA) and a Vydac 218 250mm C18 5 micron column (Vydac Grace, Columbia, Maryland, USA.) The column was heated to 40°C and proteins were eluted at flow rate of 0.2mL/min over a 120-min gradient of 0.2% TFA in acetonitrile (solvent A) and 0.2%TFA in water (solvent B). The gradient consisted of 95%–70% B in 20min, followed by 70%–40% B in 60min and 40%–20% B in 20min. Fractions were collected every 1.5min using an offline fraction

collector. The separation was performed three times and combined. Fractions were dried using a Savant SPD131DDA Speedvac Concentrator (Thermo Scientific) and reconstituted in 30 μ L of 40% acetonitrile. One μ L of each fraction was spotted for analysis by MALDI MS. Wells containing proteins of interest were targeted for top-down analysis.

LC-Coupled Tandem Mass Spectrometry

Rat brain homogenate extracts were loaded onto a reversed-phase capillary trap column using a helium-pressurized cell (pressure bomb). The trap column (360 μ m o.d. \times 150 μ m i.d.) was fitted with a filter end-fitting (IDEX Health & Science) and packed with 4cm of C8 reverse phase material (5 μ m, 300 \AA , YMC Co.). Once the sample was loaded, an M-520 microfilter union (IDEX Health & Science) was used to connect the trap column to a capillary analytical column (360 μ m o.d. \times 100 μ m i.d.), equipped with a laser-pulled emitter tip and packed with 15cm of C8 material (5 μ m, 300 \AA , YMC Co.). Using an Eksigent NanoLC Ultra HPLC, proteins were gradient-eluted at a flow rate of 500 nL/min, and the mobile phase solvents consisted of 0.1% formic acid, 99.9% water (solvent A) and 0.1% formic acid, 99.9% acetonitrile (solvent B). The gradient consisted of 5%–50% B in 55min, followed by 50%–95% B in 8 min. Upon gradient-elution, proteins were mass analyzed on an ETD-enabled LTQ Orbitrap Velos mass spectrometer, equipped with a nanoelectrospray ionization source (Thermo Scientific, San Jose, CA, USA). The instrument was operated using a data-dependent method. Full scan spectra of m/z 400–2000 (resolving power (RP): 60,000 at m/z 200) were acquired as the initial scan event per duty cycle. For data-dependent scan events, the four most abundant ions in each MS scan were selected for fragmentation using ETD in the Velos ion trap. Dynamic exclusion was enabled allowing a repeat count of 1 within 20s. ETD tandem mass spectra were acquired sequentially using the LTQ Velos ion trap followed by the Orbitrap (RP: 15,000 at m/z 200) for mass analysis. An isolation width of 3Da and an ETD reaction time of 80ms were used for MS/MS spectra. The MS^n AGC target value in the ion trap was set to 2×10^4 , the MS^n AGC target for Orbitrap scan events was 8×10^5 , and the ETD reagent ion (fluoranthene) AGC target was set to 1×10^5 . Spectra were de novo sequenced and searched using BLAST databases.

For identification of modified S100A8, the purified fraction of interest was diluted 15-fold in 0.1% formic acid. Five μ L of diluted sample were loaded for each analysis as described previously. Sequencing modified S100A8 was performed similarly to above, but the instrument method was customized with targeted scan events to assure ETD MS/MS acquisition of $[M+11H]^{11+}$ and $[M+12H]^{12+}$ charges states of modified S100A8. An isolation width of 4 m/z and an ETD reaction time of 70ms in the Velos ion trap were used for MS/MS spectra. The MS^n AGC target value in the Orbitrap was set to 7.5×10^5 , and MS/MS spectra were acquired with a resolving power of 15,000 at m/z 200. Theoretical

fragmentation data of mouse S100A8 (P27005) were generated using Protein Prospector MS-Product (v 5.12.4 <http://prospector.ucsf.edu/>). MS/MS spectra acquired over an 18-s time range (retention time 68.23–68.53min) were averaged and de novo sequenced to determine modifications. Modifications were confirmed at the peptide level following LC-MS/MS analysis of a tryptic digestion of the S100A8 fraction. An aliquot of the HPLC fraction was digested with mass-spectrometry grade endoproteinase trypsin (Promega, Madison, WI, USA.) Peptides were acidified and bomb-loaded onto a self-packed trap column (360 μ m o.d. \times 100 μ m i.d.) packed with 4cm of C18 reverse phase material (Jupiter C18, 5 μ m beads, 300 \AA ; Phenomenex). An M-520 microfilter union (IDEX Health & Science) was used to connect the trap column to a capillary analytical column (360 μ m o.d. \times 100 μ m i.d.), equipped with a laser-pulled emitter tip and packed with 18cm of C18 material (Jupiter, 3 μ m beads, 300 \AA ; Phenomenex). Using an Eksigent NanoLC Ultra HPLC, peptides were gradient-eluted at a flow rate of 500 nL/min, and the mobile phase solvents consisted of 0.1% formic acid, 99.9% water (solvent A) and 0.1% formic acid, 99.9% acetonitrile (solvent B). A 90-min gradient was performed, consisting of 2%–40% B in 75min, followed by 40%–95% B in 5min. Upon gradient elution, peptides were mass analyzed on a Q Exactive mass spectrometer. The instrument method consisted of MS^1 acquisition (RP: 70,000 at m/z 200) followed by up to 18 MS/MS scans (RP: 17,500 at m/z 200) of the most abundant ions detected in the preceding MS scan. The MS^2 AGC target value was set to 2×10^5 ions, with a maximum ion time of 150ms and a 4% underfill ratio. HCD collision energy was set to 28, dynamic exclusion was set to 10s, and peptide match and isotope exclusion were enabled. Resulting MS/MS spectra were searched against a *Mus musculus* subset database of the UniprotKB protein database using a custom version of SEQUEST (Thermo Scientific) operating on the Vanderbilt ACCRE computing cluster. Search parameters included variable modifications of oxidation (+15.9949) on methionine and oxidation of cysteine to cysteic acid (+47.9847). Search results were assembled using Scaffold 4.0 (Proteome Software, Portland, OR, USA).

Results and Discussion

Proof-of-Concept: MALDI FTICR IMS of Intact Proteins

For MALDI IMS, protein identification has traditionally been limited by poor sensitivity and fragmentation efficiency for on-tissue analysis or inadequate mass accuracy to effectively correlate imaging data with proteomics experiments using indirect identification strategies. As shown in Figure 1, MALDI FTICR IMS is capable of overcoming these challenges by producing imaging data of intact proteins with high mass resolution and accuracy. Analysis of rat brain tissue provided rich data with good sensitivity for ions up to m/z \sim 12,000 (Figure 1a). The

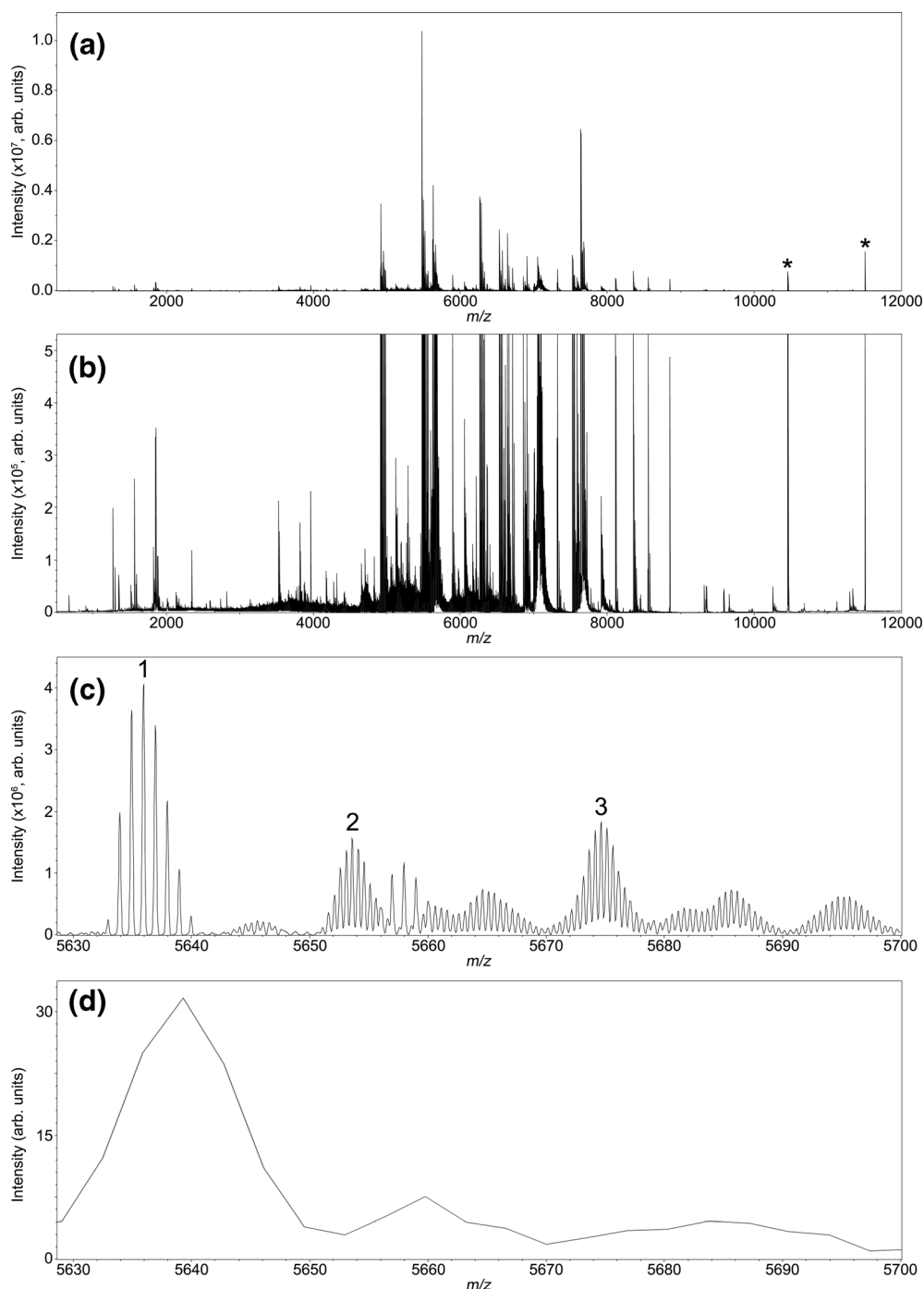


Figure 1. MALDI FTICR IMS of intact proteins from rat brain tissue. The average spectrum of the entire imaging data set is shown in (a). Expanding the intensity scale (b) highlights the overall complexity and quality of the data with singly and doubly charged protein signals detected between m/z 1000 and 12,000. Data were collected with a resolving power of $\sim 40,000$ at m/z 5000 providing isotopic resolution and allowing ions of different charge states and modifications to be distinguished (c). The ion labeled 1 is singly charged and ions labeled 2 and 3 are examples of doubly charged ions. For comparison, MALDI TOF IMS data set collected in linear mode from a serial tissue section is displayed in (d). Electronic noise peaks are labeled (*)

presented data, which are plotted as the overall average from the entire imaging experiment, were collected with a resolving power of $\sim 40,000$ at m/z 5000 resulting in 2123 peaks between m/z 2000 and 12,000 with $S/N > 20$. Expanding the intensity

scale (Figure 1b) shows the overall complexity and quality of the data. MALDI FTICR IMS provides the mass resolution necessary to distinguish protein charge states and overlapping isotopic distributions from neighboring ions (Figure 1c). The

resolving power of the experiment is more than sufficient to resolve the isotopic envelope for a given protein, enabling unambiguous assignment of charge state as demonstrated by the difference in isotope spacing between the singly charged ion labeled 1 (spacing: ~ 1.00 Da) and the doubly charged ions labeled 2 and 3 (spacing: ~ 0.501 Da). Although not all of the isotopic patterns were fully resolved, at least 10 different species can be discerned from the MALDI FTICR IMS results in just the 70Da window spanning m/z 5630–5700. It should be noted that, although at lower signal intensity, the singly charged ions of the proteins observed as doubly charged in this mass range were detected with m/z values $>10,000$. Figure 1d represents the average spectrum from a serial tissue section using MALDI TOF IMS in linear mode. These data are typical of most protein imaging experiments and clearly demonstrate the difficulty in making accurate identifications using low mass resolution IMS. Although reflectron TOF can provide higher mass resolution, linear MALDI TOF analysis was unable to resolve the complex mixture of overlapping proteoforms and proteins of differing charge states detected from rat brain tissue in this same m/z window (m/z 5630–5700). Additionally, peak shifts and broadening, likely due to surface charging or varying sample height, are clearly observed. MALDI FTICR platforms are not subject to adverse effects related to surface characteristics because the mass analyzer is decoupled from the ion source. However, TOF analyzers have a dramatic throughput advantage over FT-based platforms because pixel acquisition rates for FT instruments are generally limited by the scan time of the detection event. Although tunable, to maintain relatively high mass resolving powers, images are typically collected with scan times ranging from 0.5 to 2s, limiting acquisition rates to ~ 2 pixel/s. TOF mass analyzers equipped with high repetition rate lasers, on the other hand, are limited by ion flight times that range from ~ 10 to 200μ s and are able to rapidly produce ion images with acquisition rates that approach 10 – 30 pixel/s [44–46]. Both platforms have specific advantages for IMS

experiments, but the ability of MALDI FTICR MS to produce ion images with high mass resolution and accuracy is ideal for imaging and identifying proteins from biological tissues.

Figure 2 shows selected ion images at m/z 4,936.536 ($[M+H]^+$), m/z 4,963.502 ($[M+H]^+$), m/z 5,636.074 ($[M+H]^+$), m/z 5,653.700 ($[M+2H]^{2+}$, 11.3kDa), and m/z 5,674.720 ($[M+2H]^{2+}$, 11.4kDa). Imaging data were collected at a spatial resolution of 75μ m (pixel spacing) with $\sim 38,000$ total pixels. Even at this modest spatial resolution, substructures within the cerebellum (white matter, granular cell layer, and molecular layer) are clearly resolved. To minimize interference from overlapping isotopic patterns, images were plotted by selecting only the highest intensity isotope for each protein. Each of the presented ion images has a distinct spatial distribution within rat brain tissue. The ion at m/z 5,636.074 is detected throughout the brain; however, within the cerebellum it can be found at higher intensities in the molecular layer. Ions at m/z 5,653.700 and m/z 5,674.720 are both found to be enriched in the granular cell layer of the cerebellum and proteins detected at m/z 4,936.536 and m/z 4,963.502 are absent from the cerebellum and primarily observed to be localized to the corpus callosum. For comparison, the tissue was stained by H&E following IMS analysis. All of the ion distributions are consistent with observed structures in the microscopy image.

Proteins highlighted in Figure 2 were identified using mass accuracy as the link between MALDI FTICR IMS data and LC-ESI top-down proteomics results. All top-down experiments were performed in high mass resolution mode (resolving power: $\sim 60,000$ at m/z 200) using standard identification strategies. The protein detected at m/z 4,963.502 by MALDI FTICR IMS was identified as N-terminally acetylated thymosin β_4 ($T\beta_4$ -NtermAC, 0.1ppm). Top-down ETD data for the $[M+8H]^{8+}$ charge state of $T\beta_4$ -NtermAC (m/z 621.4440, 0.13ppm) can be found in Figure 3. The protein was determined to be acetylated on the N-terminus based on the observed mass shift of ~ 42.01 for all observed c ions. ETD spectra

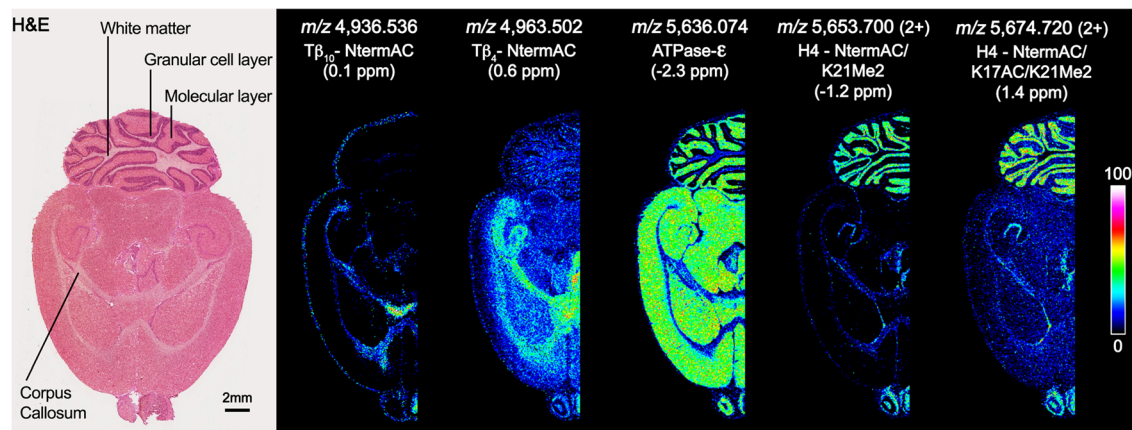


Figure 2. Selected ion images of intact proteins from rat brain tissue collected using MALDI FTICR MS. Ions were identified using mass accuracy to correlate imaging results with separate top-down proteomics experiments. For comparison, the tissue was H&E stained following IMS analysis. Doubly charged ions are indicated

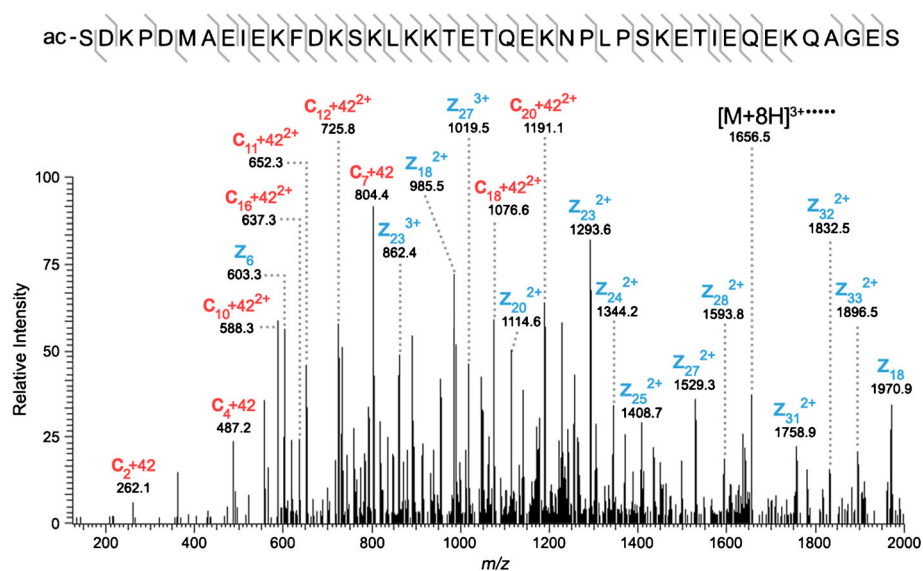


Figure 3. High mass resolution top-down ETD for the $[M+8H]^{8+}$ charge state of thymosin $\beta 4$. Selected c (red) and z (blue) ions are labeled clearly showing acetylation on the N-terminus. The amino acid sequence highlighting the fragmentation coverage is also provided

and sequence coverage summaries for all other ions can be found in [Supplementary Material](#). The ion at m/z 4,936.536 was determined to be N-terminally acetylated thymosin $\beta 10$ ($T\beta_{10}$ -NtermAC, 0.1ppm). Thymosin $\beta 4$ and $\beta 10$ are known to bind monomeric actin (G-actin) and regulate actin polymerization (F-actin). Controlled actin polymerization is essential for normal cytoskeletal function [47, 48]. The protein detected by MALDI FTICR IMS at m/z 5,636.074 was identified as mitochondrial ATP synthase subunit ϵ (ATPase- ϵ , -2.3ppm). ATPase- ϵ is a subunit of the F1 complex of ATP synthase, a 500kDa protein found in mitochondria that is critical for production of ATP [49, 50]. The MALDI ions detected at m/z 5,653.700 and m/z 5,674.720 are both doubly charged proteoforms of histone H4; the first of which, m/z 5,653.700, is acetylated at the N-terminus and the amino acid residue lysine 21 is dimethylated (H4-NtermAC/K21Me2, -1.2ppm). The ion at m/z 5,674.720 is similar but has an additional acetylation of the lysine at position 17 (H4-NtermAC/K17AC/K21Me2). Histone H4 is one of five primary histone proteins that act as the structural core of nucleosomes. Histone H4 is known to undergo extensive acetylation and methylation, which is thought to control gene expression [51, 52]. MALDI FTICR IMS provides the mass resolution and accuracy needed to differentiate the complex mixture of proteins and their associated proteoforms while enabling identifications to be made with greater confidence than with traditional MALDI TOF experiments.

Case Study: Modification of S100A8 at Infectious Foci

S. aureus is a Gram-positive pathogen that has the ability to infect virtually any organ [53]. A hallmark of *S. aureus*

infection is the formation of purulent infectious foci, called abscesses. Abscess formation has been studied extensively using histological methods and is characterized by the robust accumulation of neutrophils and macrophages. These host immune cells are equipped with a range of antimicrobial strategies [54], including the ability to induce oxidative stress [53, 55–58] in an attempt to kill pathogens. Reactive oxygen species (ROS) generated in response to pathogens can have bystander effects to host cells, sometimes causing irreparable damage and cell death.

Of particular interest is the host protein calprotectin, which accounts for an estimated 60% of the cytosolic protein content of neutrophils [40]. Calprotectin is a metal-chelating heterodimer consisting of the protein subunits S100A8 and S100A9 [41]. Bacterial pathogens proliferating within vertebrates must obtain nutrient metals from their hosts to survive and cause disease. In response, vertebrates sequester these elements from pathogens, a process known as nutritional immunity [42, 43]. Previous IMS experiments have shown that the subunits S100A8 and S100A9 have a high relative concentration at infectious foci. At these foci, calprotectin is in close proximity to other proteins known to generate ROS. However, oxidative damage to calprotectin by ROS has not been extensively characterized [59–61]. Imaging proteins with MALDI FTICR MS provides the performance necessary to spatially describe this important family of proteins, including their many proteoforms.

MALDI FTICR IMS protein data collected from kidney tissue from a mouse infected with *S. aureus* is shown in Figure 4. These data have similar figures of merit to the previously discussed rat brain analysis. The average spectrum from the entire imaging experiment shows ions detected with good sensitivity up m/z ~12,000 (Figure 4a). The data were

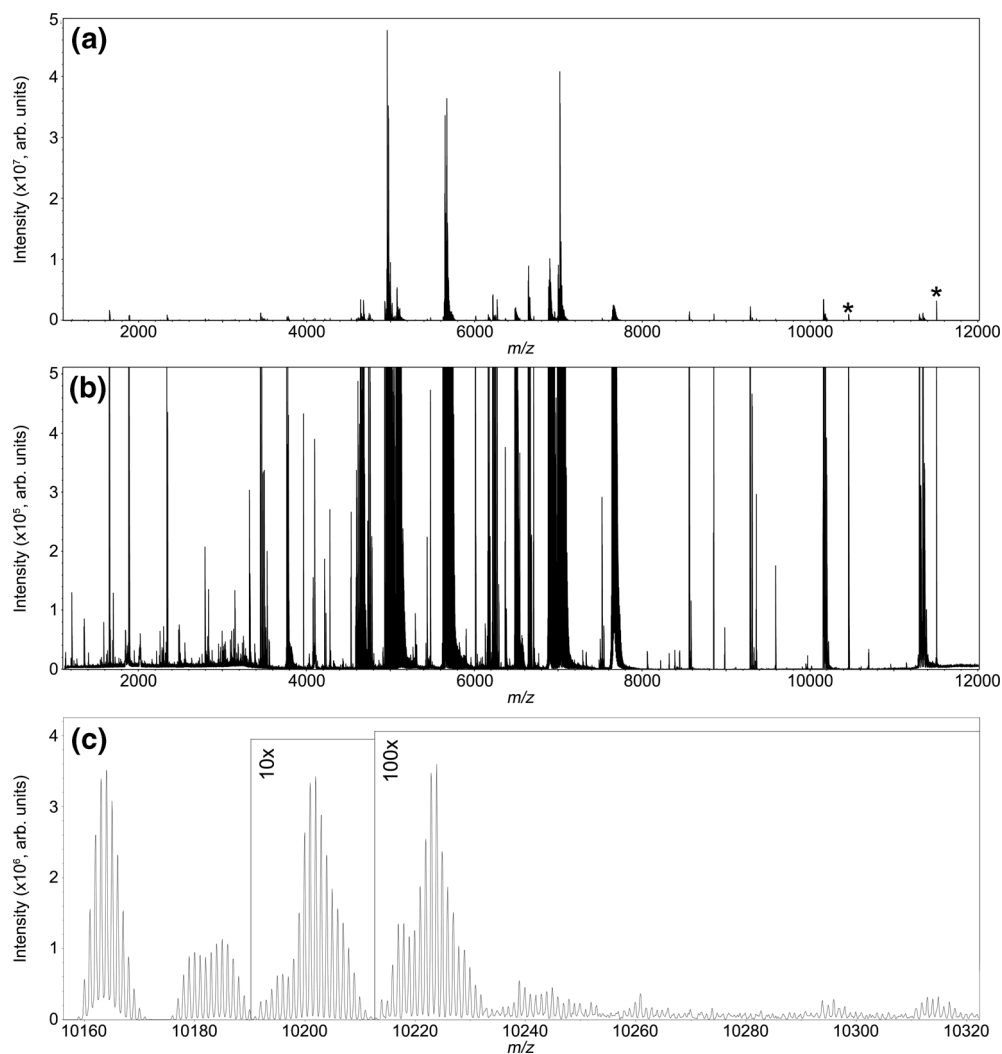


Figure 4. MALDI FTICR IMS of intact proteins from kidney tissue from a mouse infected with *S. aureus*. The average spectrum of the entire imaging data set is shown in (a). Expanding the intensity scale (b) highlights the overall quality of the data with singly and doubly charged protein signals detected between m/z 1000 and 12,000. Data were collected with a resolving power of $\sim 75,000$ at m/z 5000 providing isotopic resolution and allowing multiple isoforms of S100A8 to be distinguished (c). Electronic noise peaks are labeled (*)

collected with slightly higher resolving power, $\sim 75,000$ at m/z 5000, resulting in 2552 peaks detected between m/z 2000 and 12,000 with $S/N > 20$. To highlight the overall spectral quality provided by MALDI FTICR IMS, a view with the intensity scale expanded is provided in Panel B. The protein S100A8 was detected at m/z 10,164.03 ($[M+H]^+$, -2.1 ppm) and was identified by top-down fragmentation (Supplemental Materials). Figure 4c provides a detailed view of the mass spectrum near S100A8 from m/z 10,160 to 10,320. Although not fully resolved, the data suggest there are ~ 12 species within the highlighted mass window, all likely unique proteoforms of S100A8.

Understanding the impact of oxidative damage to S100A8 on its function during the host–pathogen interaction is of great importance. Figure 5a shows ion images for a proposed

series of oxidative modifications to S100A8. MALDI FTICR images of acetylated $T\beta_{10}$ ($T\beta_{10}$ -AC, $[M+H]^+$, 1.2ppm) and acetylated $T\beta_4$ ($T\beta_4$ -AC, $[M+H]^+$, 1.6ppm) were included for comparison. Labeled ions (*) are only tentatively identified based on mass accuracy. Both thymosins were found to localize primarily to non-abscessed tissue, whereas S100A8 and the oxidation products S100A8+O (m/z 10,180.07, $[M+H]^+$, 2.3ppm), S100A8+2O (m/z 10,196.07, $[M+H]^+$, 3.0ppm), and S100A8+4O (m/z 10,228.00, $[M+H]^+$, -2.6 ppm) were all specifically detected with greater intensity at infectious foci. An interesting observation is that oxidation seems to occur at a greater rate near the center of abscesses leading to more advanced oxidation products at these locations. This is particularly noticeable comparing the MALDI FTICR IMS data with an H&E stained micrograph of a serial

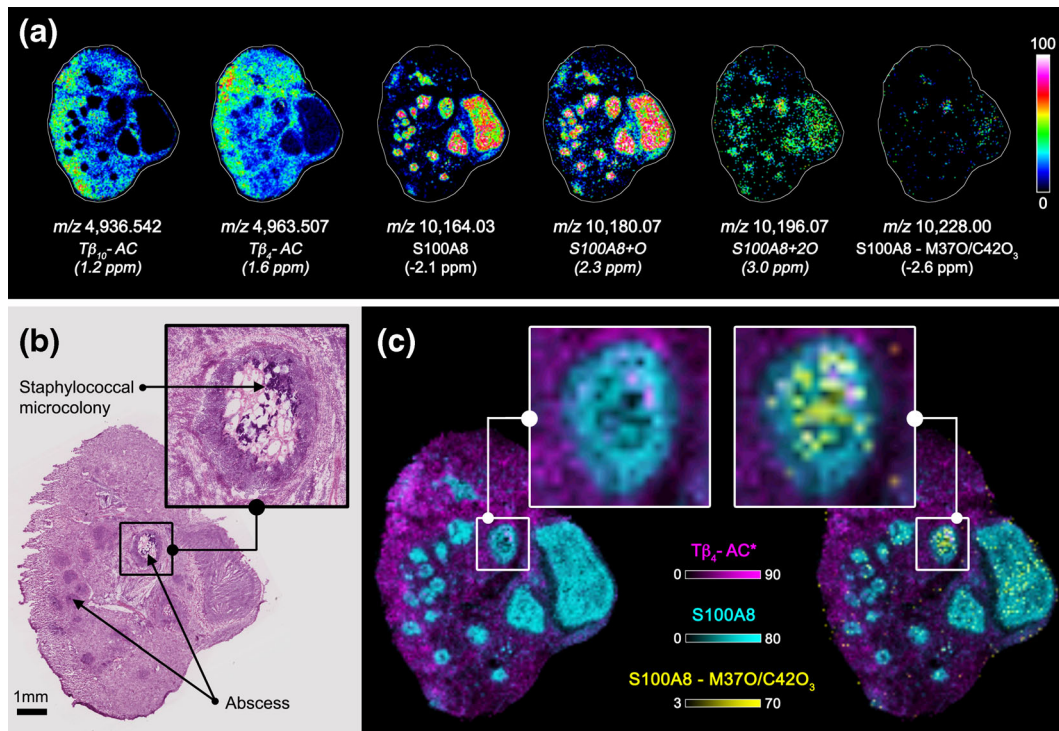


Figure 5. Selected ion images of intact proteins from kidney tissue from a mouse infected with *S. aureus* collected using MALDI FTICR MS (a). Ions were identified using mass accuracy to correlate imaging results with separate top-down proteomics experiments. For comparison, a serial tissue section was H&E stained (b). Ion image overlays show the advanced oxidation product S100A8 – M7O/C42O₃ is localized specifically to the center of infectious foci (c). Italicized ions were tentatively identified by mass accuracy only

tissue section (Figure 5b). Abscesses are clearly distinguished as darker stained regions in the microscopy image, and a zoomed-in view of one particular abscess highlights a staphylococcal microcolony that can be found at the center of these infectious foci. In comparing the histologic images to overlays of ion images (Figure 5c), advanced oxidation products are found to co-localize to regions where the staphylococcal microcolonies are found. The overlay displayed on the left side of Figure 5c shows S100A8 is localized to the infectious foci; however, the unmodified form of the protein seems to be of lower abundance at the center of the highlighted abscess. On the other hand, the S100A8+4O oxidation product, shown on the right side of Figure 5c, is found in the center of this particular abscess suggesting oxidative processes are occurring specifically at the host–pathogen interface.

To fully describe the underlying biology, it is critical to confirm that the observed ion at m/z 10,228.00 is in fact an oxidation product of S100A8 and to elucidate the amino acid residues that have been modified. Top-down ETD data for the parent ion m/z 853.260 ($[M+12H]^{12+}$) is shown in Figure 6a and observed fragment ions are summarized in the accompanying amino acid sequence (Figure 6b). Although a number of larger fragment ions contain oxidation modifications, to improve sequence coverage, bottom-up strategies were also employed (Figure 6c). The tryptic peptide highlighted in pink (Figure 6b) was fragmented and

contained two oxidized amino acid residues. De novo sequencing of both the top-down and bottom-up results found methionine 37 to be oxidized (M37O) and cysteine 42 to have its thiol modified to sulfonic acid (C42O₃). Bottom-up fragment ions of particular importance for making this identification included the b_2+16 fragment showing the addition of oxygen to methionine 37 and the b_5+16 and b_6+64 fragment ions that result from three oxygen atoms being added to cysteine 42. Oxidation of S100A8 has been hypothesized to play a critical role in the protein’s antimicrobial activity [62].

The ability to differentiate modified proteins with high confidence in MALDI FTICR IMS experiments with high resolution and mass accuracy is important to infection biology because protein modifications, such as oxidation, are hypothesized to elicit both innate and adaptive immune responses [62]. For calprotectin, which has extensive downstream effects as both an initiator of inflammation and a signaling molecule, defining the biologically relevant form of the protein becomes very important [63]. Oxidized proteoforms of S100A8 and S100A9 have previously been hypothesized to suppress inflammation [60]. Given the important biological role of calprotectin both as a major component of nutritional immunity and as a mediator of inflammatory response, IMS analyses such as these stand to greatly enhance our knowledge of calprotectin’s oxidative forms at infectious foci.

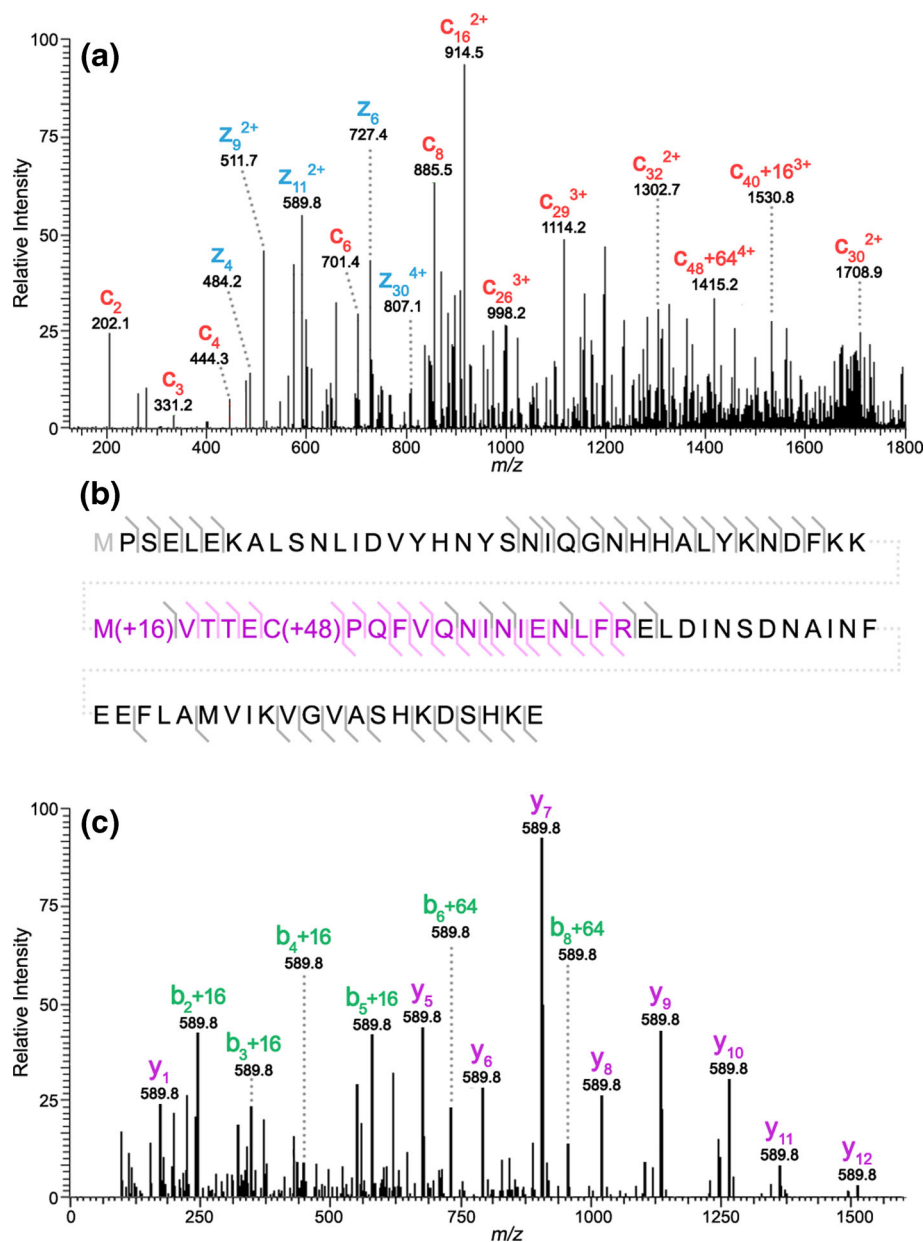


Figure 6. LC-MS/MS results for S100A8 – M370/C42O₃. (a) Shows high mass resolution top-down ETD data for the $[M+12H]^{12+}$ parent ion with selected c (red) and z (blue) ions labeled. The amino acid sequence summarizing both top-down and bottom-up fragmentation coverage is provided (b). Grey fragment ion indicators designate top-down ions and pink indicators represent bottom-up results. (c) Shows high mass resolution bottom-up fragmentation data for the tryptic peptide highlighted in pink (b). The resulting fragments clearly show oxidation to both methionine 37 (+O) and cysteine 42 (+3O)

Conclusions

Imaging mass spectrometry is a highly sensitive and efficient discovery tool used to enhance classic histologic analysis by providing specific molecular detail. However, identification of detected proteins remains a significant challenge. Indirect identification is one of the most effective strategies for identifying molecules of interest in IMS experiments. By separately performing MALDI IMS and LC-MS/MS, each can be operated optimally for their individual tasks. Previously, this

strategy has lacked sufficient mass accuracy in the imaging data to correlate the two approaches with high confidence. We have demonstrated here that MALDI FTICR MS is capable of overcoming this challenge by producing ion images with high mass resolution ($\sim 75,000$ at m/z 5000) and accuracy (<5 ppm) for proteins up to and beyond 10,000Da. Analysis of control rat brain tissue and kidney tissue from a mouse infected with *S. aureus* showed that protein charge states and complex mixtures of proteoforms were able to be distinguished, making identification more feasible and allowing these tissues to be

studied with unprecedented molecular detail. The protein identified as S100A8 – M370/C42O₃, one of ~12 modified forms of S100A8 that were detected, was found to localize with higher intensity at the center of infectious foci where staphylococcal microcolonies reside. Although further work is needed to validate this observation, it supports the hypothesis that oxidative processes are occurring specifically at the host–pathogen interface.

Detection of proteins from tissue with masses >12kDa using MALDI FTICR IMS represents a significant advancement in molecular imaging technologies; however, a vast number of endogenous proteins have even larger molecular weights. Diminished sensitivity for larger proteins is likely due to the difficulty in desorbing higher molecular weight analytes from tissue and limited ion transfer efficiencies of these analytes for many commercial source components (e.g., multipoles and ion funnels). This issue is not unique to MALDI FTICR IMS experiments, as the majority of proteins detected from tissue using MALDI-TOF platforms are typically <30kDa. Continuing to develop new methods for detecting and identifying proteins is critical to exposing the underlying biology that drives the images we collect. High mass accuracy and resolving power instrumentation enables such identifications to be made with high confidence.

Acknowledgments

The authors acknowledge support for this work by grants from the NIH/NIGMS (5 P41 GM103391-04 and 5R01 GM058008) and the National Institutes of Health Shared Instrumentation Grant Program (1S10OD012359-01) awarded to R.M.C. and the National Institute of Allergy and Infectious Diseases (R01 AI101171-01A1 and R21 AI107233) awarded to E.P.S.D.G.R. is supported by the Aegis Sciences Fellowship in Chemistry, Vanderbilt University. J.L.M. is supported by Vanderbilt Chemical Biology Interface training program (T32 GM 065086) and the Mitchum Warren Graduate Research Fellowship. N.D.H. is a CF Foundation Ann Weinberg Memorial Research Fellow. The authors also thank Dr. Junhai Yang, Dr. Dhananjay Sakrikar, Salisha Hill M.S., and Amanda Hachey for their technical support.

References

1. Caprioli, R.M., Farmer, T.B., Gile, J.: Molecular imaging of biological samples: localization of peptides and proteins using MALDI-TOF MS. *Anal. Chem.* **69**, 4751–4760 (1997)
2. Nilsson, A., Goodwin, R.J., Shariatgorji, M., Vallianatou, T., Webborn, P.J., Andren, P.E.: Mass spectrometry imaging in drug development. *Anal. Chem.* **87**, 1437–1455 (2015)
3. Huang, J.T., Hannah-Qiuhua, L., Szyszka, R., Veselov, V., Reed, G., Wang, X., Price, S., Alquier, L., Vas, G.: Molecular imaging of drug-eluting coronary stents: method development, optimization and selected applications. *J. Mass Spectrom.* **47**, 155–162 (2012)
4. Bhandari, D.R., Schott, M., Rompp, A., Vilcinskas, A., Spengler, B.: Metabolite localization by atmospheric pressure high-resolution scanning microprobe matrix-assisted laser desorption/ionization mass spectrometry imaging in whole-body sections and individual organs of the rove beetle *Paederus riparius*. *Anal. Bioanal. Chem.* **407**, 2189–2201 (2015)
5. Berry, K.A., Hankin, J.A., Barkley, R.M., Spraggins, J.M., Caprioli, R.M., Murphy, R.C.: MALDI imaging of lipid biochemistry in tissues by mass spectrometry. *Chem. Rev.* **111**, 6491–6512 (2011)
6. Groseclose, M.R., Andersson, M., Hardesty, W.M., Caprioli, R.M.: Identification of proteins directly from tissue: in situ tryptic digestions coupled with imaging mass spectrometry. *J. Mass Spectrom.* **42**, 254–262 (2007)
7. Schober, Y., Guenther, S., Spengler, B., Rompp, A.: High-resolution matrix-assisted laser desorption/ionization imaging of tryptic peptides from tissue. *Rapid Commun Mass Spectrom.* **26**, 1141–1146 (2012)
8. Deutschens, F., Yang, J., Caprioli, R.M.: High spatial resolution imaging mass spectrometry and classical histology on a single tissue section. *J. Mass Spectrom.* **46**, 568–571 (2011)
9. Seeley, E.H., Schwamborn, K., Caprioli, R.M.: Imaging of intact tissue sections: moving beyond the microscope. *J. Biol. Chem.* **286**, 25459–25466 (2011)
10. Smith, L.M., Kelleher, N.L., The Consortium for Top Down Proteomics: Proteoform: a single term describing protein complexity. *Nat. Methods* **10**, 186–187 (2013)
11. Zhang, Y., Fonslow, B.R., Shan, B., Baek, M.C., Yates III, J.R.: Protein analysis by shotgun/bottom-up proteomics. *Chem. Rev.* **113**, 2343–2394 (2013)
12. Schwartz, S.A., Weil, R.J., Johnson, M.D., Toms, S.A., Caprioli, R.M.: Protein profiling in brain tumors using mass spectrometry: feasibility of a new technique for the analysis of protein expression. *Clin. Cancer Res.* **10**, 981–987 (2004)
13. Balluff, B., Rauser, S., Meding, S., Elsner, M., Schone, C., Feuchtinger, A., Schuhmacher, C., Novotny, A., Jutting, U., Maccarone, G., Sarioglu, H., Ueffing, M., Braselmann, H., Zitzelsberger, H., Schmid, R. M., Hofler, H., Ebert, M. P., Walch, A.: MALDI imaging identifies prognostic seven-protein signature of novel tissue markers in intestinal-type gastric cancer. *Am. J. Pathol.* **179**, 2720–2729 (2011)
14. Kelleher, N.L.: Top-down proteomics. *Anal. Chem.* **76**, 197A–203A (2004)
15. Inutan, E.D., Richards, A.L., Wager-Miller, J., Mackie, K., McEwen, C.N., Trimpin, S.: Laserspray ionization, a new method for protein analysis directly from tissue at atmospheric pressure with ultrahigh mass resolution and electron transfer dissociation. *Mol. Cell. Proteom.* **10**, M110.000760 (2011)
16. Trimpin, S., Inutan, E.D., Herath, T.N., McEwen, C.N.: Laserspray ionization, a new atmospheric pressure MALDI method for producing highly charged gas-phase ions of peptides and proteins directly from solid solutions. *Mol. Cell Proteome* **9**, 362–367 (2010)
17. Kiss, A., Smith, D.F., Reschke, B.R., Powell, M.J., Heeren, R.M.: Top-down mass spectrometry imaging of intact proteins by laser ablation ESI FT-ICR MS. *Proteomics* **14**, 1283–1289 (2014)
18. Nemes, P., Vertes, A.: Laser ablation electrospray ionization for atmospheric pressure, in vivo, and imaging mass spectrometry. *Anal. Chem.* **79**, 8098–8106 (2007)
19. Takats, Z., Wiseman, J.M., Gologan, B., Cooks, R.G.: Mass spectrometry sampling under ambient conditions with desorption electrospray ionization. *Science* **306**, 471–473 (2004)
20. Robichaud, G., Barry, J.A., Garrard, K.P., Muddiman, D.C.: Infrared matrix-assisted laser desorption electrospray ionization (IR-MALDESI) Imaging source coupled to a FT-ICR mass spectrometer. *J. Am. Soc. Mass Spectrom.* **24**, 92–100 (2013)
21. Robichaud, G., Barry, J.A., Muddiman, D.C.: IR-MALDESI mass spectrometry imaging of biological tissue sections using ice as a matrix. *J. Am. Soc. Mass Spectrom.* **25**, 319–328 (2014)
22. Gessel, M.M., Norris, J.L., Caprioli, R.M.: MALDI imaging mass spectrometry: spatial molecular analysis to enable a new age of discovery. *J. Proteome* **17**, 71–82 (2014)
23. Mascini, N.E., Heeren, R.M.A.: Protein identification in mass-spectrometry imaging. *Trac-Trend Anal. Chem.* **40**, 28–37 (2012)
24. Schey, K.L., Anderson, D.M., Rose, K.L.: Spatially-directed protein identification from tissue sections by top-down LC-MS/MS with electron transfer dissociation. *Anal. Chem.* **85**, 6767–6774 (2013)
25. Marshall, A.G., Hendrickson, C.L., Jackson, G.S.: Fourier transform ion cyclotron resonance mass spectrometry: a primer. *Mass Spectrom. Rev.* **17**, 1–35 (1998)
26. Zubarev, R.A., Makarov, A.: Orbitrap mass spectrometry. *Anal. Chem.* **85**, 5288–5296 (2013)
27. Makarov, A.: Electrostatic axially harmonic orbital trapping: a high-performance technique of mass analysis. *Anal. Chem.* **72**, 1156–1162 (2000)

28. Wang, X., Han, J., Pan, J., Borchers, C.H.: Comprehensive imaging of porcine adrenal gland lipids by MALDI-FTMS using quercetin as a matrix. *Anal. Chem.* **86**, 638–646 (2014)
29. Cornett, D.S., Frappier, S.L., Caprioli, R.M.: MALDI-FTICR imaging mass spectrometry of drugs and metabolites in tissue. *Anal. Chem.* **80**, 5648–5653 (2008)
30. Minerva, L., Boonen, K., Menschaert, G., Landuyt, B., Baggerman, G., Arckens, L.: Linking mass spectrometric imaging and traditional peptidomics: a validation in the obese mouse model. *Anal. Chem.* **83**, 7682–7691 (2011)
31. Schober, Y., Schramm, T., Spengler, B., Rompp, A.: Protein identification by accurate mass matrix-assisted laser desorption/ionization imaging of tryptic peptides. *Rapid Commun Mass Spectrom.* **25**, 2475–2483 (2011)
32. Manier, M.L., Spraggins, J.M., Reyzer, M.L., Norris, J.L., Caprioli, R.M.: A derivatization and validation strategy for determining the spatial localization of endogenous amine metabolites in tissues using MALDI imaging mass spectrometry. *J. Mass Spectrom.* **49**, 665–673 (2014)
33. Corbin, B.D., Seeley, E.H., Raab, A., Feldmann, J., Miller, M.R., Torres, V.J., Anderson, K. L., Dattilo, B. M., Dunman, P. M., Gerads, R., Caprioli, R. M., Nacken, W., Chazin, W. J., Skaar, E. P.: Metal chelation and inhibition of bacterial growth in tissue abscesses. *Science* **319**, 962–965 (2008)
34. Attia, A.S., Schroeder, K.A., Seeley, E.H., Wilson, K.J., Hammer, N.D., Colvin, D.C., Manier, M. L., Nicklay, J. J., Rose, K. L., Gore, J. C., Caprioli, R. M., Skaar, E. P.: Monitoring the inflammatory response to infection through the integration of MALDI IMS and MRI. *Cell Host Microbe* **11**, 664–673 (2012)
35. Hood, M.I., Mortensen, B.L., Moore, J.L., Zhang, Y., Kehl-Fie, T.E., Sugitani, N., Chazin, W. J., Caprioli, R. M., Skaar, E. P.: Identification of an *Acinetobacter baumannii* zinc acquisition system that facilitates resistance to calprotectin-mediated zinc sequestration. *PLoS Pathog.* **8**, e1003068 (2012)
36. Kehl-Fie, T.E., Zhang, Y., Moore, J.L., Farrand, A.J., Hood, M.I., Rath, S., Chazin, W. J., Caprioli, R. M., Skaar, E. P.: MntABC and MntH contribute to systemic *Staphylococcus aureus* infection by competing with calprotectin for nutrient manganese. *Infect Immun* **81**, 3395–3405 (2013)
37. Mike, L.A., Dutter, B.F., Stauff, D.L., Moore, J.L., Vitko, N.P., Aranmolate, O., Kehl-Fie, T. E., Sullivan, S., Reid, P. R., DuBois, J. L., Richardson, A. R., Caprioli, R. M., Sulikowski, G. A., Skaar, E. P.: Activation of heme biosynthesis by a small molecule that is toxic to fermenting *Staphylococcus aureus*. *Proc. Natl. Acad. Sci. U. S. A.* **110**, 8206–8211 (2013)
38. Moore, J.L., Becker, K.W., Nicklay, J.J., Boyd, K.L., Skaar, E.P., Caprioli, R.M.: Imaging mass spectrometry for assessing temporal proteomics: analysis of calprotectin in *Acinetobacter baumannii* pulmonary infection. *Proteomics* **14**, 820–828 (2014)
39. Moore, J.L., Caprioli, R.M., Skaar, E.P.: Advanced mass spectrometry technologies for the study of microbial pathogenesis. *Curr. Opin. Microbiol* **19**, 45–51 (2014)
40. Clohessy, P.A., Golden, B.E.: Calprotectin-mediated zinc chelation as a biostatic mechanism in host defence. *Scand J Immunol* **42**, 551–556 (1995)
41. Steinbakk, M., Naess-Andresen, C.F., Lingaas, E., Dale, I., Brandtzaeg, P., Fagerhol, M.K.: Antimicrobial actions of calcium binding leucocyte L1 protein, calprotectin. *Lancet* **336**, 763–765 (1990)
42. Hood, M.I., Skaar, E.P.: Nutritional immunity: transition metals at the pathogen-host interface. *Nat Rev Microbiol* **10**, 525–537 (2012)
43. Kehl-Fie, T.E., Skaar, E.P.: Nutritional immunity beyond iron: a role for manganese and zinc. *Curr. Opin. Chem. Biol.* **14**, 218–224 (2010)
44. Trim, P.J., Djidja, M.C., Atkinson, S.J., Oakes, K., Cole, L.M., Anderson, D.M., Hart, P. J., Francese, S., Clench, M. R.: Introduction of a 20 kHz Nd:YVO4 laser into a hybrid quadrupole time-of-flight mass spectrometer for MALDI-MS imaging. *Anal. Bioanal. Chem.* **397**, 3409–3419 (2010)
45. Spraggins, J.M., Caprioli, R.M.: High-speed MALDI-TOF imaging mass spectrometry: rapid ion image acquisition and considerations for next generation instrumentation. *J. Am. Soc. Mass Spectrom* **22**, 1022–1031 (2011)
46. Prentice, B.M., Chumbley, C.W., Caprioli, R.M.: High-speed MALDI MS/MS imaging mass spectrometry using continuous raster sampling. *J. Mass Spectrom* **50**, 703–710 (2015)
47. Siripala, A.D., Welch, M.D.: SnapShot: actin regulators II. *Cell* **128**, 1014 (2007)
48. Siripala, A.D., Welch, M.D.: SnapShot: actin regulators I. *Cell* **128**, 626 (2007)
49. von Ballmoos, C., Wiedenmann, A., Dimroth, P.: Essentials for ATP synthesis by F1F0 ATP synthases. *Annu Rev Biochem* **78**, 649–672 (2009)
50. Habersetzer, J., Ziani, W., Larrieu, I., Stines-Chaumeil, C., Giraud, M.F., Brethes, D., Dautant, A., Paumard, P.: ATP synthase oligomerization: from the enzyme models to the mitochondrial morphology. *Int. J. Biochem. Cell Biol.* **45**, 99–105 (2013)
51. Luger, K., Mader, A.W., Richmond, R.K., Sargent, D.F., Richmond, T.J.: Crystal structure of the nucleosome core particle at 2.8 Å resolution. *Nature* **389**, 251–260 (1997)
52. Arnaudo, A.M., Garcia, B.A.: Proteomic characterization of novel histone post-translational modifications. *Epigenetics Chromatin* **6**, 24 (2013)
53. Cheng, A.G., DeDent, A.C., Schneewind, O., Missiakas, D.: A play in four acts: *Staphylococcus aureus* abscess formation. *Trends Microbiol* **19**, 225–232 (2011)
54. Russell, D.G.: *Staphylococcus* and the healing power of pus. *Cell Host Microbe* **3**, 115–116 (2008)
55. Cheng, A.G., Kim, H.K., Burts, M.L., Krausz, T., Schneewind, O., Missiakas, D.M.: Genetic Requirements for *Staphylococcus aureus* abscess formation and persistence in host tissues. *FASEB J.* **24**, 3393–3404 (2009)
56. Thammavongsa, V., Missiakas, D.M., Schneewind, O.: *Staphylococcus aureus* degrades neutrophil extracellular trapsto promote immune cell death. *Science* **342**, 863–866 (2013)
57. Buckley, C.D., Gilroy, D.W., Serhan, C.N., Stockinger, B., Tak, P.P.: The resolution of inflammation. *Nat. Rev. Immunol.* **13**, 59–66 (2013)
58. Farrera, C., Fadeel, B.: Macrophage clearance of neutrophil extracellular traps is a silent process. *J. Immunol.* **191**, 2647–2656 (2013)
59. Attia, A.S., Cassat, J.E., Aranmolate, S.O., Zimmerman, L.J., Boyd, K.L., Skaar, E.P.: Analysis of the *Staphylococcus aureus* abscess proteome identifies antimicrobial host proteins and bacterial stress responses at the host–pathogen interface. *Pathog. Dis.* **69**, 36–48 (2013)
60. Lim, S.Y., Raftery, M.J., Geczy, C.L.: Oxidative modifications of DAMPs suppress inflammation: the case for S100A8 and S100A9. *Antioxid Redox Signal* **15**, 2235–2248 (2011)
61. Gomes, L.H., Raftery, M.J., Yan, W.X., Goyette, J.D., Thomas, P.S., Geczy, C.L.: S100A8 and S100A9-oxidant scavengers in inflammation. *Free Radic. Biol. Med.* **58**, 170–186 (2013)
62. Ryan, B.J., Nissim, A., Winyard, P.G.: Oxidative post-translational modifications and their involvement in the pathogenesis of autoimmune diseases. *Redox. Biol.* **2**, 715–724 (2014)
63. Ehrchen, J.M., Sunderkötter, C., Foell, D., Vogl, T., Roth, J.: The endogenous Toll-like receptor 4 agonist S100A8/S100A9 (calprotectin) as innate amplifier of infection, autoimmunity, and cancer. *J. Leukoc. Biol.* **86**, 557–566 (2009)